BULLETIN OF THE EARTHQUAKE
RESEARCH INSTITUTE
Vol. 48 (1970), pp. 707-727

38. *Focal Process of a Deep Focus Earthquake as Deduced from Long Period P and S Waves.*

By Yoshio FUKAO,*

Earthquake Research Institute.

(Read Jan. 27, 1970.—Received July 15, 1970.)

Abstract

The focal process of a deep shock which occurred at 580 km depth in the Banda Sea region in 1964 is investigated by using long period P and S waves from WWSSN seismograms. The two nodal planes of this earthquake are given by dip direction=319°, dip angle=45°, and dip direction=180°, dip angle=53°, respectively. Assuming that a rectangle represents a far field pulse form, the S wave seismograms are synthesized for various pulse widths and epicentral distances. The effects on the wave form due to passage through the mantle, crust and instrument are removed. Trials are made to find the pulse width, T_s, of the original rectangular pulse which fits the observed S wave form. The variation of T_s with respect to the fault plane orientation is investigated. T_s is remarkably well correlated with the emergence angle measured from the slip vector on the nodal plane with dip direction=319°, dip angle=45°. This result leads to the following conclusions: (1) The source is plane-like rather than spherical; a fault model is more preferable to a phase transition model. (2) The nodal plane with dip direction=319° and dip angle=45° is the fault plane. (3) The fault surface is not circular but elongated. (4) The direction of elongation coincides with the slip direction. (5) The fault width W should not exceed 15 km. It may probably be smaller than 10 km. (6) The fault length L is estimated to be 40 km. (7) The process of the body wave radiation took place almost simultaneously, within about two seconds, over the entire fault surface; this model is significantly different from the ordinary propagating fault model. On the basis of this model, the seismic moment M_0 is estimated to be 5.8×10^{26} dyne cm from the P wave amplitude and width. Assuming W=8 km, the average dislocation, stress drop and elastic energy released when the fault surfaces become free, are estimated to be 150 cm, 290 bars and 7.0×10^{22} ergs, respectively. The stress drop obtained here is one order of magnitude greater than that estimated for shallow earthquakes.

* Graduate Student, Communicated by S. Miyamura.

1. Introduction

It appears from first motion and amplitude studies that almost all earthquakes are shear failures. For shallow earthquakes it is almost certain that these are slippages on pre-existing fault planes. For deep shocks, however, two different mechanisms have been proposed. The first is similar to that of shallow earthquakes i.e. Coulomb-Navier type brittle fracture (Raleigh and Paterson, 1965; Isacks *et al.* 1968; McKenzie, 1969a, b; Isacks and Molnar, 1969), and the second includes some instability of shear flow which becomes catastrophic and concentrated more or less on one plane (Orowan, 1961, 1965; Griggs and Baker, 1968; Savage, 1969).

Because of its lower speed, the S wave is expected to be more strongly affected by the source than the P wave. We will first investigate the variation of the S wave form with the fault plane orientation. The results may answer such questions as:

(1) Which is the preferable source model: spherical origin or plane source?

(2) If the latter is preferable, which one of the two P nodal planes is the fault plane and what is the shape of the fault surface?

(3) What are the source dimensions?

(4) How long is the source time duration?

The answer to (1) provides a key for testing the phase change hypothesis and those to (3) and (4) for testing the propagating fault model. In order to check the results derived from S wave data, and to determine some important physical quantities, such as the seismic moment, stress drop and elastic energy released, the pulse form and the absolute amplitude of P waves will be investigated.

Few investigations of the focal process have been made in the time domain (Bollinger, 1968; Berckhemer and Jacob, 1968; Mikumo, 1969). Bollinger (1968) related the time duration of the P pulse radiated from an assumed propagating fault to that of the observed P wave record in order to find the fault length and rupture velocity. Our method is similar to his but the propagating fault is not a priori assumed as the source model.

2. Focal coordinates and mechanism solution

A deep focus earthquake in the Banda Sea region was chosen for the present study. The focal coordinates, according to the Bulletin of the International Seismological Center (ISC), are as follows.

Date: Oct. 18, 1964 Time: 12h 32m 24.9s GMT

Table 1. Station list and pertinent data.

Station	Δ deg.	Azimuth deg.	Back Azimuth deg.	First Motions of *P* or *PKP*	i_d for *P* or *PKP* deg.	*pP* First Motions	i_d for *pP* deg.
AAE	86.4	279.5	97.6	−	28.5		
ADE	30.9	156.1	330.7	+	57.8		
AFI	63.4	102.0	269.1	−	39.1		
AQU	109.9	312.4	81.2	−	26.0	+	154.0
ARE	149.1	146.8	214.5	−	9.0		
ATL	141.6	41.1	308.7	−	10.0		
ATU	102.4	307.2	89.2	−	26.3	+	154.0
BAG	23.5	351.7	171.5	+	63.0		
BEC	150.1	16.6	340.4	−	8.7		
BHP	152.3	83.6	273.1	−	8.0		
BKS	113.0	51.9	279.3	−	25.7		
BLA	141.4	32.9	317.5	−	10.0		
LEM	16.3	269.6	182.9	+	73.0		
BOZ	118.6	41.3	261.7	−	25.5		
BUL	92.6	249.5	98.4	−	27.0		
CAR	168.7	71.4	287.0	−	3.5		
CHG	35.6	316.5	133.8	+	55.3		
CMC	107.8	20.0	296.6	−	26.3		
COL	95.5	153.5	265.4	−	26.8		
COP	107.8	326.5	281.2	−	26.3	+	154.0
CTA	25.2	123.3	298.0	+	61.2		
DAV	14.1	6.4	186.4	+	78.8		
DUG	119.5	47.5	287.2	−	26.0		
ESK	116.2	329.5	61.8	−	26.0	+	154.0
GEO	141.7	27.8	323.6	−	10.0		
GIE	143.4	101.3	256.8	−	10.0		
GUA	29.1	45.5	226.7	−	59.0		
HKC	30.7	341.9	160.6	+	57.8		
HLW	95.7	299.3	94.7	−	26.6	+	152.8
HNR	35.6	96.4	271.1	−	55.0		
HOW	45.6	310.9	125.8	+	49.8		
IST	98.3	310.4	92.0	−	26.3	+	153.5
JER	92.6	301.5	96.6	−	27.0	+	151.7
KEV	98.9	339.5	85.9	−	26.0	+	154.0
KIP	81.5	67.2	259.1	−	30.2		
LAH	61.0	311.9	120.1	−	40.5	+	136.8
LPS	144.8	74.7	291.4	−	9.7		
MAN	21.7	352.4	172.2	+	64.5		
MUN	25.1	195.9	18.5	+	61.5		
NAI	87.1	269.1	96.9	−	28.3	+	150.0

(to be continued)

Table 1

(continued)

Station	Δ deg.	Azimuth deg.	Back Azimuth deg.	First Motions of P or PKP	i_d for P or PKP deg.	pP First Motions	i_d for pP deg.
NDI	57.4	310.5	120.8	−	42.0	+	132.3
NNA	149.0	132.2	228.7	−	9.0		
NDR	103.5	354.5	40.3	−	26.3	+	154.0
NUR	100.7	330.2	85.3	−	26.3	+	154.0
OGD	141.1	23.2	328.3	−	10.0		
GSC	117.7	53.8	281.7	−	25.5		
PMG	23.0	97.5	274.2	−	63.3		
POO	55.6	298.0	112.5	−	43.5	+	129.0
PRE	92.1	243.9	98.8	−	27.0	+	151.8
QUE	66.0	307.3	114.2	−	38.0	+	138.3
QUI	152.2	106.8	251.9	−	8.5		
RAB	28.2	85.8	263.0	−	59.5		
RIV	36.6	140.5	310.6	+	55.0	−	118.0
SBA	74.2	171.4	315.5	−	34.0	+	143.0
SCP	140.1	26.8	323.9	−	10.0		
SEO	44.4	3.4	184.2	−	50.8	−	124.0
SHA	140.7	47.8	301.4	−	10.0		
SHI	77.3	302.5	105.7	−	32.5	+	145.0
SJG	165.2	40.9	316.9	−	4.5		
ANP	32.1	355.8	175.4	+	57.3		
TRI	109.1	315.9	80.2	−	27.2		
TRN	173.5	55.4	303.7	−	2.0		
WIN	102.7	245.1	103.2	−	26.0		
TSK	45.6	18.3	202.7	−	49.8	−	124.8

The positive sign of the initial motion means the vertical upward motion (Compression) and the negative sign the downward (Dilatation).

Latitude: 7.17°S Longitude: 123.86°E
Depth: 585 km (575 km from pP) Magnitude: 6.9 (Rothé, 1969)

Records were obtained from long period instruments of the world-wide standard network and that of TSK. The data on which the first-motion studies were based are listed in Table 1. The determination of the P wave first motions is unambiguous, since the consistency among the three components is confirmed. Readings of the clear first motion of the pP phase are also tabulated in Table 1; pP phases were successfully used by Hedayati and Hirasawa (1966) for focal mechanism determinations. To avoid the complexity of the phase shift of the reflected wave near the cusp (Shimamura and Sato, 1965), readings of the pP

phase were made only for $\Delta \gtrsim 35$. The angles of incidence, i_d, of P and pP waves at the focus are taken from $(i-\Delta)$ curves of Ritsema (1958). The observations are plotted in Fig. 1, using the equal area projection of the lower half of the focal sphere. The unique solution indicated by the solid curves in Fig. 1 is obtained visually so that all the data of the P and pP phases are consistent with the solution. In the plots of pP data a symmetrical push-pull pattern with respect to the origin was assumed. Two P nodal planes are given by ($\alpha=319°$, $\delta=45°$) and ($\alpha=180°$, $\delta=53°$) where α and δ are the dip direction and dip angle of a nodal plane. In an alternative representation, the dip angle$=45°$, the slip angle$=121°40'$ and the strike azimuth$=49°$. According to Ben-Menahem *et al.* (1968) who made a spectral analysis of P waves for the mechanism determination of the same earthquake, the dip angle$=43°$ and the slip angle$=118°$, which closely agree with the present results. The radiation pattern of S waves supports the double couple assumption.

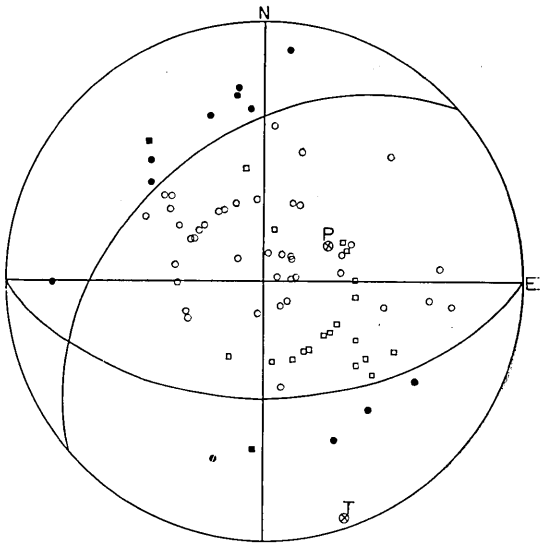

Fig. 1. Fault plane solution.
filled circle: compression (from P wave)
open circle: dilatation (from P wave)
filled square: compression (from pP wave)
open square: dilatation (from pP wave)

3. Method

An earthquake is considered as a sudden transition in a shear field from one equilibrium state to another accompanied by a sudden wave energy release. The elastic forces which result from this transition should be of more or less step-wise time dependence. The elastic waves generated by this kind of forces have, in the first approximation, the form of a rectangular pulse in the far field; the width of the pulse is governed by the finiteness of the source and the rise time of the energy release. The detailed structure of the wave form certainly depends on the rupture process (e.g. Savage, 1966) but the mantle and other transit effects will make such details insignificant on a seismogram. We define a unit rectangular pulse, $f(t)$, by

$$f(t)=H(t)-H(t-T) \tag{1}$$

where $H(t)$ is a unit step function. Define a complex function $F(\omega)$ as

$$\begin{aligned} F(\omega)&=\int_{-\infty}^{\infty} f(t)e^{-i\omega t}dt \\ &=\frac{i}{\omega}(e^{-i\omega T}-1)\,. \end{aligned} \tag{2}$$

If we consider the mantle-crust-instrument system as a linear filter, the output signal $g(t)$, i.e. the observed body wave signal, is written as

$$g(t)=\frac{1}{2\pi}\int_{-\infty}^{\infty} D(\omega)F(\omega)e^{i\omega t}d\omega \tag{3}$$

where $D(\omega)$ is the complex transfer function of the filter. According to Ben-Menahem *et al.* (1965), $D(\omega)$ is given by

$$D(\omega)=D_M(\omega)D_{CR}(\omega)D_{INS}(\omega) \tag{4}$$

in which $D_M(\omega)$, $D_{CR}(\omega)$ and $D_{INS}(\omega)$ are the complex transfer functions for the mantle, crust and instrument respectively. $D_M(\omega)$ can be expressed as a product of two physically distinct factors:

$$D_M(\omega)=G\times D_{AN}(\omega) \tag{5}$$

where G is a factor due to geometrical spreading and $D_{AN}(\omega)$ represents the amplitude and phase distortion caused by the anelasticity of the mantle. G can be calculated from the Jeffreys-Bullen tables but $D_{AN}(\omega)$ is only incompletely known. The amplitude distortion is given by the frequency dependent attenuation coefficient $\alpha(\omega)$ while the phase distortion is determined by the dispersion relation $k=k(\omega)$ where k is the wave number. According to Futterman (1962), these are analytically related in the causal sense in a linear theory of wave propagation.* If we write $D_{AN}(\omega)$ as:

$$D_{AN}(\omega)=e^{-\alpha(\omega)R}e^{ik(\omega)R} \tag{6}$$

then, αR and kR are related to each other as follows in a convenient form

$$\begin{aligned} \alpha k&=\frac{\omega\tau}{2Q} \\ kR&=\omega\tau\left(1-\frac{1}{\pi Q}\ln\gamma\frac{\omega}{\omega_0}\right) \qquad (\gamma\simeq 1.8) \end{aligned} \tag{7}$$

where Q is the dimensionless quality factor and ω_0 is a finite, arbitrarily

* His theory was experimentally supported by Wuenschel (1965).

Table 2. Crustal model used for the calculation of the transfer function. Standard continental crust.

	Thickness	*P* velocity	*S* velocity	Density
1st layer	11.0 km	6.10 km/sec	3.50 km/sec	2.70 g/cm^3
2nd layer	9.0	6.40	3.68	2.90
3rd layer	18.0	6.70	3.94	2.90
Half space		8.15	4.75	3.30

small but nonzero cutoff frequency below which no attenuation is assumed. Here, we take $\omega_0=0.001\ \mathrm{sec}^{-1}$. τ can be estimated from τ_0, the travel time of the body wave, rather crudely by the iteration procedure up to $n=3$.

$$\frac{1}{\tau^{(n+1)}}=\frac{1}{\tau^{(n)}}\left[1-\frac{1}{\pi Q}\left(1+\ln\frac{2\gamma Q}{\omega_0\tau^{(n)}}\right)\right]$$
$$\tau^{(0)}=\tau_0 \qquad (8)$$

The transfer function $D_{CR}(\omega)$ for a crustal model given by Table 2 was calculated by using Haskell's matrix method (Haskell, 1960, 1962). The body wave phase velocity was obtained by differentiating the travel time curve. Crustal structures were assumed to be the same for all stations because the differences in crustal structures do not produce significant differences in the form of the long period body wave seismograms. The transfer function $D_{INS}(\omega)$ was calculated according to Hagiwara's (1958) formula. The USCGS standard seismograph is assumed to have a pendulum period $T_0=30$ sec, galvanometer period $T_g=100$ sec, damping constant of pendulum $h_0=1.0$, damping constant of galvanometer $h_g=1.0$ and a coupling constant $\sigma=0.15$. For TSK which does not belong to the USCGS network, $T_0=15$ sec and $T_g=90$ sec are used.

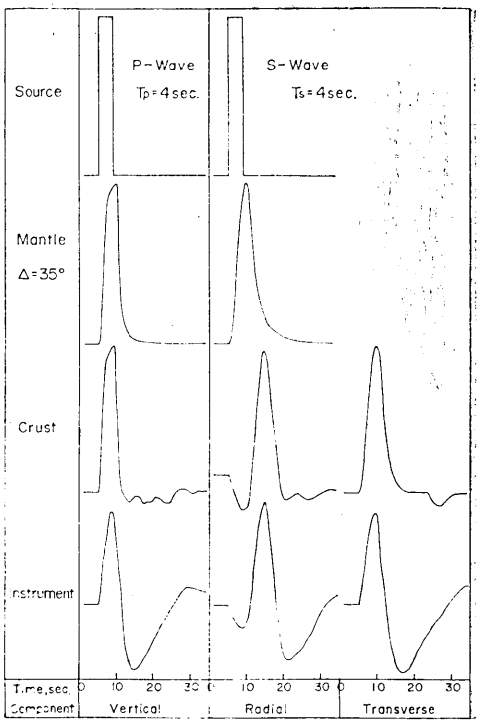

Fig. 2. Pulse distortion due to the passage through the mantle, crust and instrument.

The result of the above operations are illustrated in Fig. 2 for the focal depth $h=580$ km, epicentral distance $\Delta=35°$ and the pulse width $T=4$ sec. The Q value was assumed as 500 and 300 for P and S waves respectively. This assumption is appropriate in the range $30°<\Delta<60°$ for the focal depth of this order (Kovach and Anderson, 1964; Kanamori, 1967). The transmitted body wave forms through all the filters are given in the lowest column in Fig. 2. We constructed such theoretical S wave seismograms for various Δ and T; Δ was varied from 25° to 75° with 10° intervals and T from 2 to 12 sec at 2 sec increments. Trials were made to find an original rectangalar pulse which fits the observed S wave form. The pulse width thus found was denoted by T_s.

4. Data analysis, S wave

The analysis was made on the two horizontal components which were, whenever possible, decomposed into the transverse and radial components (T- and R-component). The signals were digitized at a rate of one point per second at all stations. These digital wave forms were all normalized so as to have the same maximum amplitude. The distance was limited to a range $\Delta<75°$ to avoid a possible contamination by ScS or SKS

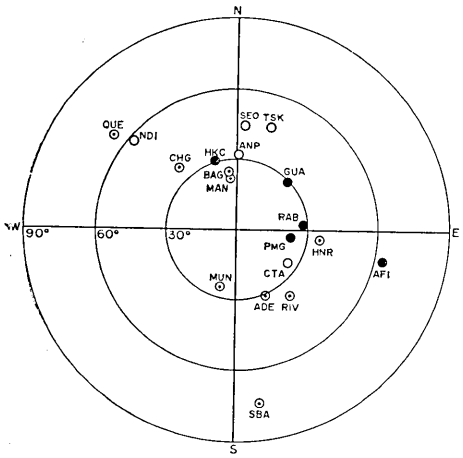

Fig. 3. Spatial distribution of stations used for the analysis, with respect to the epicenter
filled circle: station used for P wave analysis
open circle: station used for S wave analysis
double circle: station used for P and S wave analysis

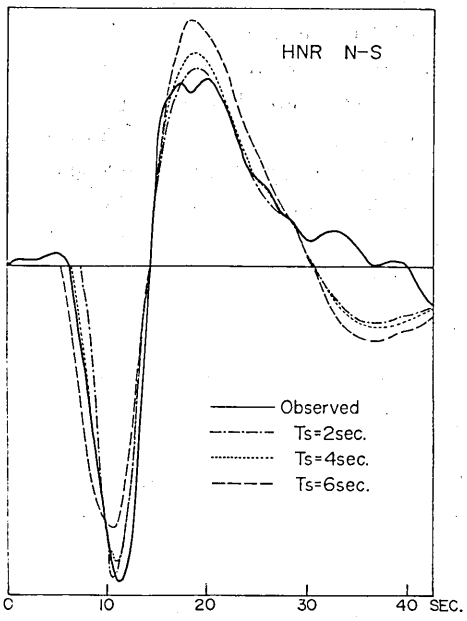

Fig. 4. Determination of T_s in the time domain. Record is from the NS-component of HNR.

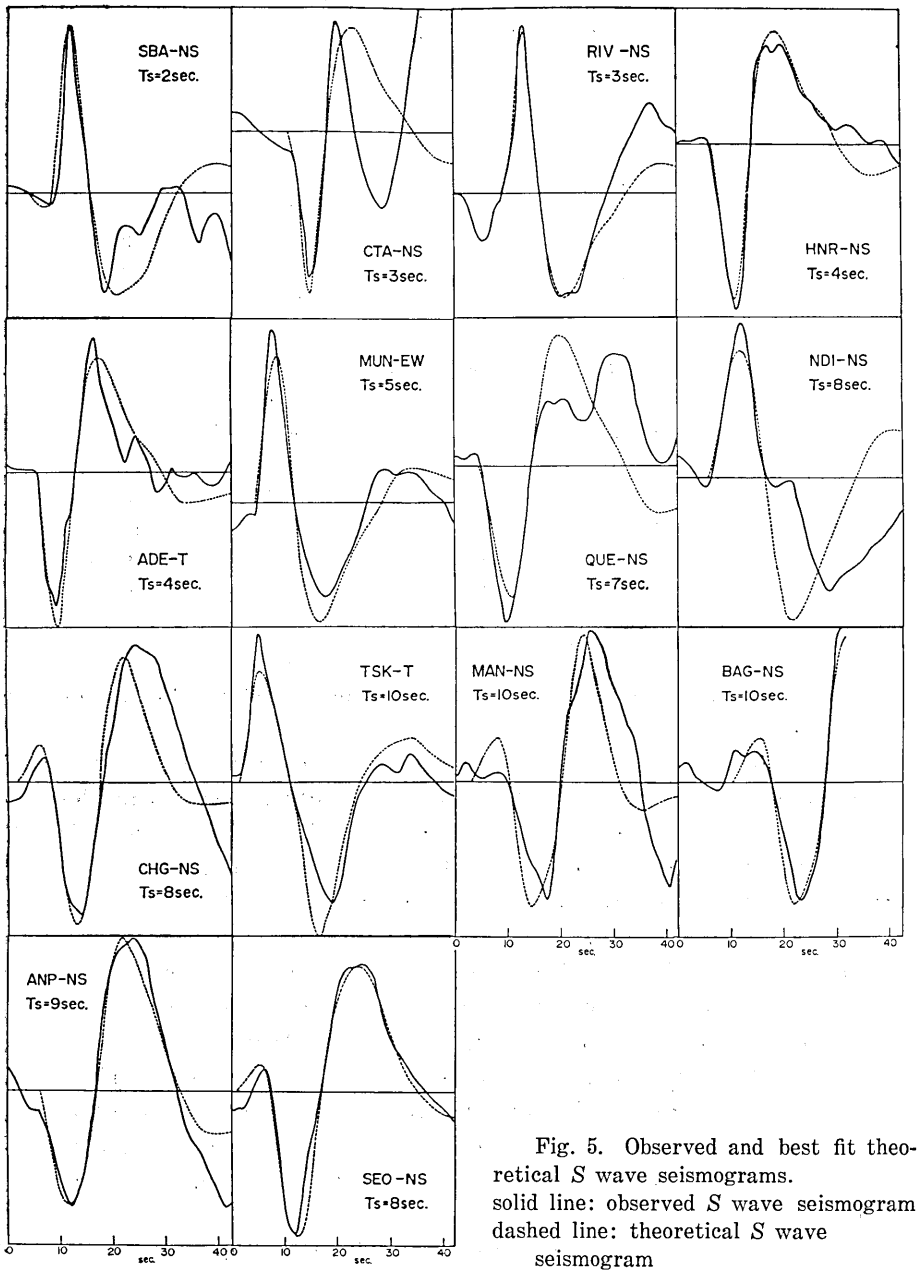

Fig. 5. Observed and best fit theoretical S wave seismograms.
solid line: observed S wave seismogram
dashed line: theoretical S wave seismogram

Table 3. Pulse width, T_s, deduced from the S wave analysis and the angles Θ, θ and ϕ for the stations used.

Station	Θ (deg)	θ (deg)	ϕ (deg)	Ts (sec)
SBA	23.2	93.8	67.1	2
CTA	20.6	84.8	109.7	3
RIV	9.9	81.0	94.1	3
HNR	33.9	105.7	119.2	4
ADE	18.4	72.9	83.7	4
MUN	47.5	67.8	51.3	5
QUE	82.4	140.5	51.5	7~8
NDI	87.2	142.5	52.6	8
CHG	100.3	144.9	56.8	8
TSK	81.8	165.7	101.6	10
MAN	103.5	166.4	89.2	10
BAG	102.0	167.7	87.8	10
ANP	95.2	174.9	88.6	8~9
SEO	86.6	176.4	91.1	8

Θ, θ and ϕ are defined in Fig. 6.

phase. The spatial distribution of the stations used in the present analysis is shown in Fig. 3.

Fig. 4 shows an example of the S wave records, taken from the NS component of HNR ($\Delta=35.6°$). It represents a pure SH motion since the station to epicenter azimuth is nearly 270°. The theoretical SH wave seismograms with different pulse widths (2, 4 and 6 sec) are compared with the observed record. It is evident that $T_s=4$ sec is most appropriate. In general T_s can be determined with an uncertainty of less than ± 1 sec. In Fig. 5 all the available S wave forms are superimposed by theoretical seismograms thus obtained. The results are summarized in Table 3; T_s varies over a wide range, from 2 to 10 sec. Such a large variation of T_s cannot be attributed to the regional difference of the propagating medium. It must be attributed to an asymmetric character of the source. Since an asymmetric radiation is a characteristic of a fault model and not of a spherical origin, we will adopt a fault model in the following.

First we shall attempt to determine which P nodal plane is the fault plane and what is the shape of the fault surface. Suppose tentatively that the nodal plane with ($\alpha=319°$, $\delta=45°$) is the fault plane. We will consider the width of the pulse which is radiated to a point P (see Fig. 6) from a rupture over a finite plane. Let the position of P be specified by a vector r in Cartesian coordinates (Fig. 6). The z axis is taken

normal to the fault plane and the x axis parallel to the slip vector on this plane. The angles between r and z-, x- and y-axis are denoted Θ, θ and ϕ respectively. If the fault surface is circular and the rupture occurs radially symmetrically, T_s depends only on Θ as

$$T_s = T_0 + T_e \sin\Theta \qquad (9)$$

(Vvedenskaya, 1959; Savage, 1966). If it is elongated in such a way that the width W is much smaller than the length L (see Fig. 6), T_s approximately depends only on θ as

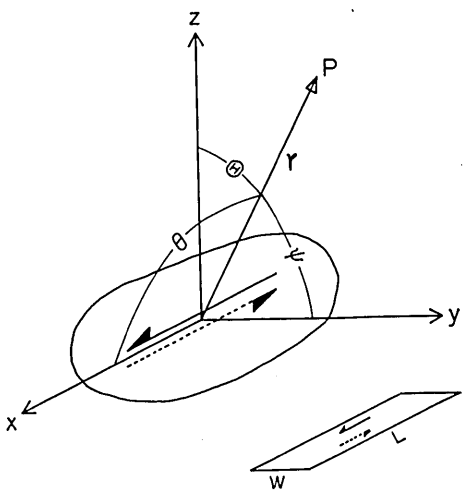

Fig. 6. Geometry of the source.

$$T_s = T_0 + T_e \cos\theta \qquad (10)$$

for a unilateral fault or

$$T_s = T_0 + T_e |\cos\theta| \qquad (11)$$

for a bilateral fault where the direction of elongation is assumed to be parallel to the slip vector. The neglected term here is

$$\frac{W}{\beta}\cos\phi \qquad (12)$$

where β is the velocity of S wave (Berckhemer and Jacob, 1965). This term arises from the finite width of the fault plane.

For a unilateral propagating fault

$$T_0 = \frac{L}{v}, \qquad T_e = \frac{L}{\beta} \qquad \text{in (10)}$$

while for a bilateral propagating fault

$$T_0 = \frac{L}{2v}, \qquad T_e = \frac{L}{2\beta} \qquad \text{in (11)}$$

(Berckhemer and Jacob, 1965). In both cases the rupture velocity v is obtained from T_0 and T_e as

$$v = \beta\frac{T_e}{T_0} \qquad (13)$$

In Figs. 7 and 8 we have plotted T_s against $\sin\Theta$ and $|\cos\theta|$ respectively. Although the points lie nearly on a straight line in both

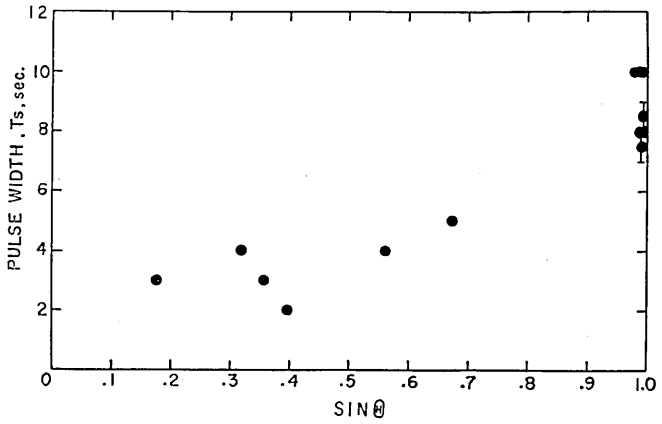

Fig. 7. Pulse width, T_s, plotted against $\sin\Theta$.

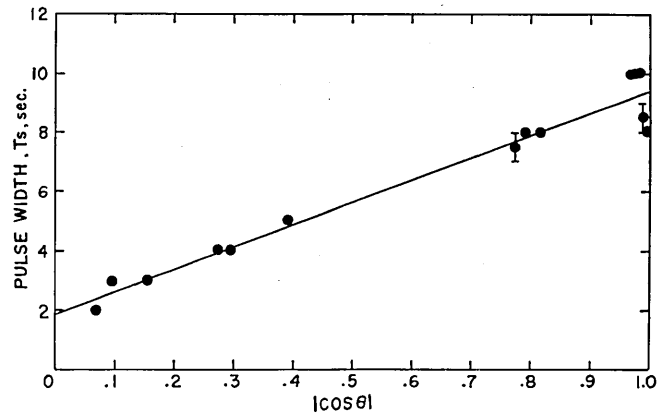

Fig. 8. Pulse width, T_s, plotted against $|\cos\theta|$.

plots, the fit of the straight line to the data is much more remarkable in Fig. 8 than in Fig. 7. This result favors an elongated fault model rather than a circular model. The results have also justified the choice of the fault plane and the direction of elongation. The least squares fit gives $T_0=1.9$ sec and $T_e=7.5$ sec in Fig. 8. Here we can roughly estimate the upper limit of the fault width W from the fact that the contribution from it expressed by (12) is negligibly small as compared with T_0: W should not exceed 15 km and may probably be smaller than 10 km.

Putting the values obtained here into (13), leads to an unreasonably high rupture velocity of 20 km/sec. Thus neither unilateral nor bilateral propagating fault is appropriate, unless the rupture velocity is unreasonably large. We would prefer the interpretation that the process of the body wave radiation took place almost simultaneously, within about

two seconds, over the entire fault surface. T_s at a point P is the difference between the arrival times of the first and last S waves; the first S wave is considered to come from the nearest point faulted at the initiation of the rupture process and the last from the farthest point faulted at the termination. T_0 is the total time duration during the faulting while, according to our interpretation, T_e is approximately equal to the time required for the S wave to propagate along the fault surface from one edge to the other. The fault length L is estimated to be 40 km as a product of T_e and $\beta=5.4$ km/sec.

5. Data analysis, P wave

If the preceding interpretation is correct, the width of the original P wave pulse, T_p, must have a form

$$T_p=T_0+\frac{L}{\alpha}|\cos\theta| \tag{14}$$

where α is the velocity of the P wave (here, taken as 10 km/sec). In Fig. 9 we compare the observed P wave forms with the theoretical P wave seismograms with the pulse width of T_p. For comparison, theoretical P seismograms with the pulse width of T_s are also shown. It is evident that T_p is much more appropriate than T_s for the pulse width of P wave. The difference between the original wave form of P and S waves is a direct evidence for the finite size of the source. The agreement between the theory and observation of the P wave form enables us to estimate the seismic moment from the amplitude.

The finiteness of the source affects the amplitude as well as the pulse width; if the P wave displacement at a distance R from the source is written in the form of a rectangular pulse as follows:

$$u(t)=\frac{1}{4\pi\rho}\frac{1}{\alpha^3}\frac{C}{R}2\cos\theta\cos\Theta[H(\tau)-H(\tau-T_p)] \tag{15}$$

where $\tau=t-(R/\alpha)$, then the "normalized pulse height" C depends on θ. Here $2\cos\theta\cos\Theta$ represents the familiar radiation pattern due to the double couple point source.

According to Haskell (1964), the P wave displacement from a fault on which the relative displacement is $D(x, t)$ is given by

$$u(t)=\frac{1}{4\pi\rho}\frac{1}{\alpha^3}\frac{\mu}{R}2\cos\theta\cos\Theta\iint_S\dot{D}(x,\tau)ds \tag{16}$$

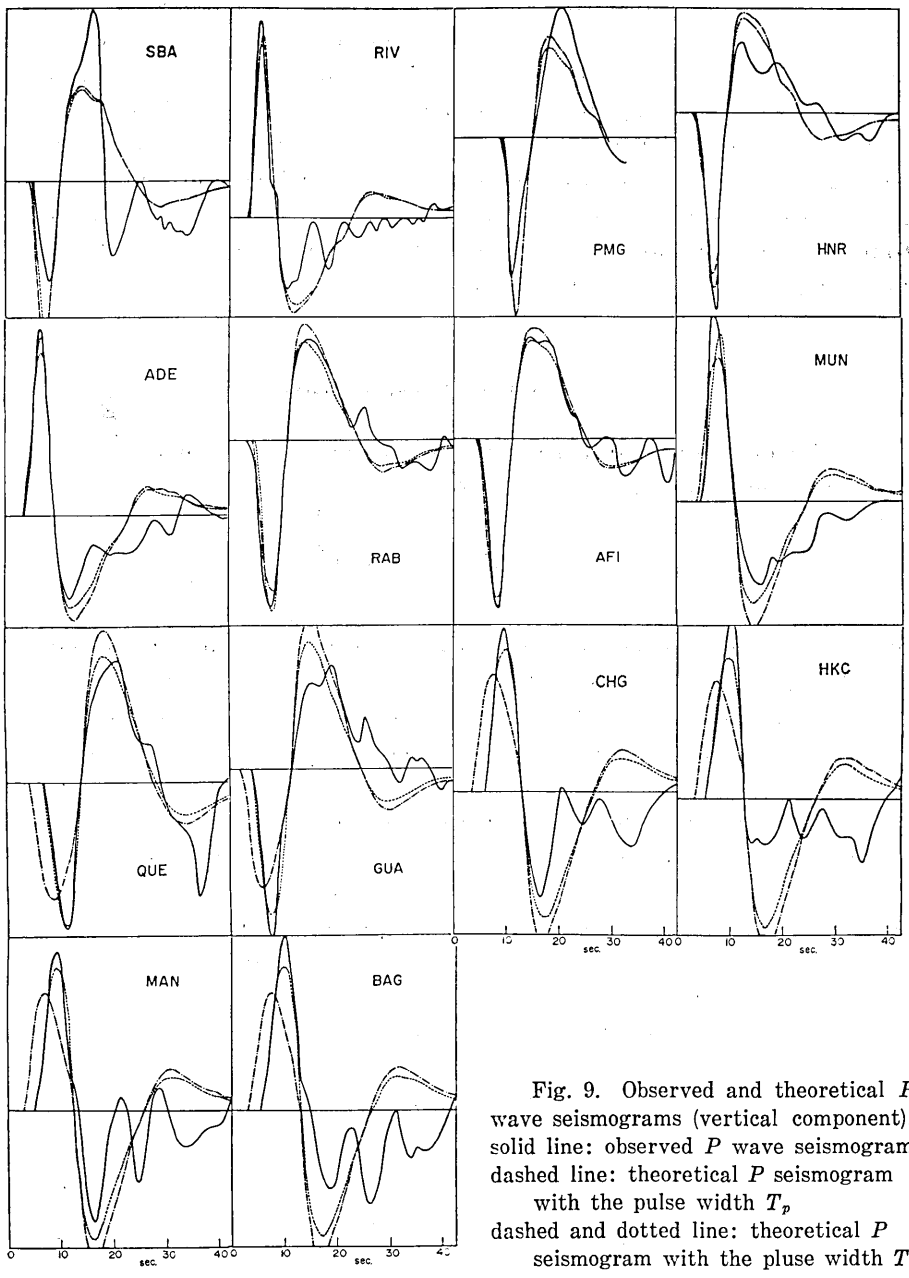

Fig. 9. Observed and theoretical P wave seismograms (vertical component).
solid line: observed P wave seismogram
dashed line: theoretical P seismogram with the pulse width T_p
dashed and dotted line: theoretical P seismogram with the pluse width T_s

where S is the fault surface, x the space coordinates on the fault, μ-the rigidity, and the dot is used to indicate the time derivative. From the equivalence of a shear dislocation along a fault to a double couple in the absence of the fault,

$$M(x, t)=\mu D(x, t) \tag{17}$$

can be considered as the spatial density of the moment of the equivalent double couple. Comparison of (15) with (16) yields

$$\iint_S \dot{M}(x, \tau)ds=C[H(\tau)-H(\tau-T_p)] \tag{18}$$

Then the seismic moment M_0 defined by

$$M_0=\int_{-\infty}^{\infty} dt \iint_S \dot{M}(x, t)ds \tag{19}$$

is given by

$$M_0=C\cdot T_p \tag{20}$$

On the other hand, from (17) and (19)

$$M_0=\mu \bar{D} S \tag{21}$$

where $\bar{D}$ is the average displacement over the fault surface.

We computed the theoretical seismogram from a rectangular pulse $H(t)-H(t-T_p)$ by making corrections for the attenuation, geometrical

Table 4. Normalized pulse height, C, and seismic moment, M_0 estimated from the P wave analysis.

Station	θ, deg	T_p, sec	C, dyne·cm/sec	M_0, dyne·cm
SBA	93.8	2.2	2.5×10^{26}	5.5×10^{26}
RIV	81.0	2.5	3.5	8.8
PMG	100.3	2.6	1.4	3.6
HNR	105.7	3.0	1.9	5.6
ADE	72.9	3.1	2.4	7.5
RAB	111.0	3.4	0.98	3.3
AFI	111.2	3.4	1.4	4.8
MUN	67.8	3.5	1.3	4.6
QUE	140.5	5.1	1.6	8.0
GUA	142.3	5.1	1.1	5.8
CHG	144.9	5.3	1.1	5.6
HKC	164.4	5.8	1.5	8.5
MAN	166.4	5.9	1.0	5.9
BAG	167.7	5.9	0.68	4.0

Ave. $=5.8\times10^{26}$

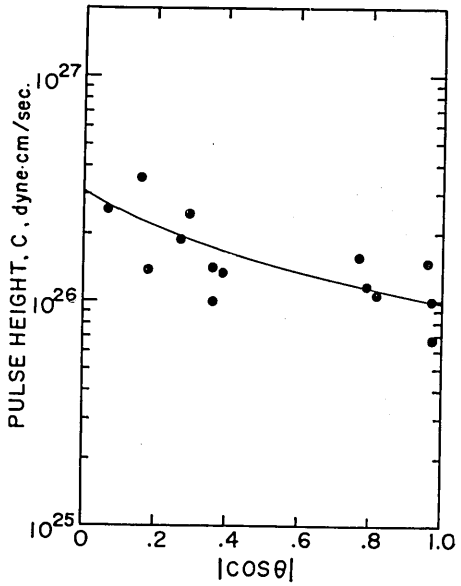

Fig. 10. Relationship between normalized pulse height, C, and $|\cos\theta|$.

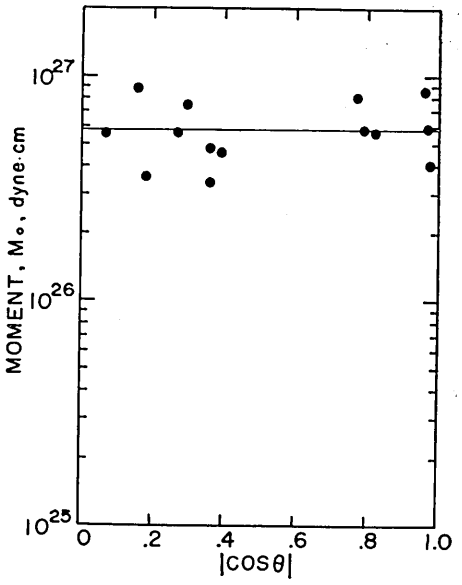

Fig. 11. Relationship between $M_0=C\cdot T_p$ and $|\cos\theta|$.

spreading, mantle-crust transmission and instrument. The normalized pulse height C can thus be estimated by

$$C=\frac{4\pi\rho\alpha^3}{2\cos\theta\cos\Theta}\frac{A_{obs}}{A_{th}} \tag{22}$$

Here A_{obs} and A_{th} are the amplitudes of the first half cycle of the P wave on the actual record and that on the theoretical seismogram. The values of C estimated for each station are tabulated in Table 4.* C is found to decrease with $|\cos\theta|$ (Fig. 10) but $M_0=C\cdot T_p$ is nearly constant with $|\cos\theta|$ (Fig. 11). This result suggests that the finite fault model assumed above is reasonable. The average seismic moment is obtained as $M_0=5.8\times10^{26}$ dyne cm.

If the static dislocation theory is applied to the present case, the shear stress drop σ parallel to the fault is related to $\bar{D}$ as

$$\sigma=\frac{4\mu}{\pi W}\bar{D} \tag{23}$$

(Knopoff, 1958). When the surfaces of the fault become free, the difference between the elastic energies of the medium without and with the fault can be written as

* Stations for which $2\cos\theta\cos\Theta\ \angle 0.1$ were discarded in the P analysis because the amplitude is too small to estimate C.

$$E_w=\frac{\pi}{8\mu}W^2L\sigma^2 \tag{24}$$

If the stress does not drop to zero on the fault surfaces, the released elastic energy should be larger than E_w (Savage, 1969). For the present earthquake $\bar{D}=150$ cm, $\sigma=290$ bars and $E_w=7.0\times10^{22}$ ergs are obtained from (19), (23) and (24) ($\mu=1.2\times10^{12}$ dyne/cm^2 is assumed).

6. Discussion

Sudden phase transition as a source for deep focus earthquakes has been proposed by Evison (1963, 1967), Benioff (1963, 1964), Randall (1964, 1966, 1968), Dennis and Walker (1965, 1968) and Walker and Dennis (1966). Honda (1959, 1962) also postulated a kind of phase transition model which explains the double couple radiation pattern. Randall's (1966) shear distortion model can also explain this pattern. Because the phase transformation is a volumetric phenomenon, a spherical seismic orgin is usually assumed. The regular azimuthal variation of T_s that we found, however, cannot be explained in terms of the spherical origin; it can be explained in terms of a source concentrated on a plane. This result favors the fault model rather than the phase transition model.

The mean value of T_p of the signals observed at randomly distributed stations on a focal sphere is

$$\bar{T}_p=\int_0^{\pi/2}T_p\sin\theta d\theta=T_0+\frac{T_e}{2} \tag{25}$$

If the signals were analyzed under the assumption of a point source whose temporal variation is given by a ramp function of time constant τ, then τ may be obtained as close to $\bar{T}_p$. In our case $\bar{T}_p=4.0$ sec. Teng and Ben-Menahem (1965) investigated a deep focus earthquake ($h=350$ km) by a spectral analysis of P wave. The spectrums were interpreted in terms of a double couple point source with a time constant $\tau\lesssim3$ sec and the seismic moment $M_0=\mu\bar{D}S=1.1\times10^{26}$ dyne cm. Mikumo (1969) compared the synthetic P seismograms with the observed P wave records for four intermediate earthquakes ($h=100\sim200$ km). He obtained $\tau\lesssim3$ sec and $M_0=1.6\sim3.0\times10^{26}$ dyne cm.* Such a small value of τ for the seismic moment of this magnitude seems to be in good harmony with our results ($\bar{T}_p=4.0$ sec and $M_0=5.8\times10^{26}$ dyne cm). The sharp pulse-like wave form from deep shocks may probably result from the rapidity of the process but not necessarily from the smallness of the source. Actually $L=40$

* The values in Mikumo's (1969) Table 4 should be multiplied by 1/2.9 for DLW, M_0, σ, ε and E_0 and by 2.9 for C and $\bar{\sigma}C$. (Mikumo, private communication).

km is so large that the fault surface cannot be formed within 2 seconds if a rupture is assumed to propagate along its longer side.

Savage (1966) postulated a circular fault surface for a deep earthquake from energy considerations: the elastic energy change per unit area of fault surface before and after the slippage is greater for a circular surface than for any other elliptical surfaces in a homogeneous medium. From the dynamical point of view, however, the fault will tend to grow more rapidly in one of the two directions, along and across the the direction of the slip, so that the fault surface will be elongated (Frank, 1965). Burridge (1968) suspected that a circular crack is unrealistic under an initial uniform shear stress because the limiting rupture velocities are different for plane strain and for antiplane strain. Our conclusion on the shape of the origin seems consistent with these latter ideas.

We obtained 290 bars for the stress drop. This value appears to be one order of magnitude larger than that estimated for zones of shallow earthquakes (Brune and Allen, 1967) but one order of magnitude smaller than the tectonic stress acting in deep earthquake zones expected from the plate theory (McKenzie, 1969b). Mikumo (1969) estimated the lower limit of the stress drop to be 55～97 bars for the four intermediate earthquakes. The stress drop accompanied by a sudden wave energy release may be smaller than the total stress drop on the fault surface and it should be smaller than the initial tectonic stress in the neighbour hood of the fault. According to the analysis of Wyss and Brune (1969), the apparent shear stresses (efficiency times average stress) reach the maximum of about 1 kbar around a depth of 100 km and those for very deep earthquakes are of the same order as the stresses for shallow earthquakes, i.e. a few tens of bars. Further studies are undoubtedly necessary concerning the release of tectonic stress.

7. Conclusions

The S wave form is very useful for the study of focal processes. From the P wave study alone, we could not reach the conclusions obtained in this study. The method and the results are summarized as follows:

1. From the S wave records we determined the width of the original rectangular pulse. A regular variation of the pulse width was found with respect to the fault plane orientation. A spherical seismic origin is obviously inappropriate.
2. From this results we estimated the slip plane, the shape of the fault surface, the upper limit of the fault width, the source time duration

and the fault length. Faulting took place almost simultaneously, within about two seconds, over the entire fault surface.

3. P wave forms were also interpreted in terms of the source model with the same parameters as for S waves. From the amplitude study of P waves the seismic moment was estimated to be 5.8×10^{26} dyne cm. Other source parameters estimated here are: average dislocation=150 cm; stress drop=290 bars; released elastic energy when the fault surfaces become free=7.0×10^{22} ergs.

Acknowledgment

I would like to express my sincere thanks to Prof. H. Kanamori for his constructive criticism and suggestions throughout this work. I am also grateful to Profs. T. Mikumo and S. Uyeda for their helpful discussions and for critically reading the manuscript.

References

BENIOFF, H., 1963. Source wave forms of three earthquakes, *Bull. Seismol. Soc. Am.*, **53**, 893-903.

BENIOFF, H., 1964. Earthquake source mechanism, *Science*, **143**, 1399-1406

BEN-MENAHEM, A., H. JAROSCH, and M. ROSENMAN, 1968. Large scale processing of seismic data in search of regional and global stress patterns, *Bull. Seismol. Soc. Am.*, **58**, 1899-1932.

BEN-MENAHEM, A., S. W. SMITH, and T. L. TENG, 1965. A procedure for source studies from spectrums of long-period seismic body waves, *Bull. Seismol. Soc. Am.*, **55**, 203-235.

BERCKHEMER, H., and K. H. JACOB, 1965. Synthetic seismic pulses from propagating faults, *Univ. Frankfurt/Main, Sci. Rept., No. 7, AF 61(052)-891*, pp. 31.

BERCKHEMER, H., and K. H. JACOB, 1968. Investigation of the dynamical process in earthquake foci by analyzing the pulse shape of body waves, *Univ. Frankfurt/Main, Sci. Rept., No. 13, AF 61(052)-801*, pp. 85.

BOLLINGER, G. A., 1968. Determination of earthquake fault parameters from long-period P waves, *J. Geophys. Res.*, **73**, 785-807.

BRUNE, J. N., and C. R. ALLEN, 1967. A low-stress-drop, low-magnitude earthquake with surface faulting: the Imperial, California, Earthquake of March 4, 1966, *Bull. Seismol. Soc. Am.*, **57**, 501-514.

BURRIDGE, R., 1968. Theoretical seismic sources and propagating brittle cracks, *J. Phys. Earth*, **16**, Special Issue, 83-92.

DENNIS, J. G., and C. T. WALKER, 1965. Earthquakes resulting from metastable phase transitions, *Tectonophys.*, **2**, 401-407,

DENNIS, J. G., and C. T. WALKER, 1968. Hypocentral patterns near island arcs, *J. Geophys. Res.*, **73**, 1506-1507.

EVISON, F. F., 1963. Earthquakes and faults, *Bull. Seismol. Soc. Am.*, **53**, 873-891.

EVISON, F. F., 1967. On the occurrence of volume change at the earthquake source, *Bull. Seismol. Soc. Am.*, **57**, 9-25.

FRANK, F. C., 1965. On dilatancy in relation to seismic sources, *Rev. Geophys.*, **3**, 485-503.

FUTTERMAN, W. I., 1962. Dispersive body waves, *J. Geophys. Res.*, **67**, 5279-5291.

GRIGGS, D. T., and D. W. BAKER, 1968. The origin of deep-focus earthquakes; in *Properties of matter*, John Wiley, New York.

HAGIWARA, T., 1958. A note on the theory of the electromagnetic seismograph, *Bull. Earthquake Res. Inst. Tokyo Univ.*, **36**, 139-164.

HASKELL, N. A., 1960. Crustal reflection of plane *SH* waves, *J. Geophys.Res.*, **65**, 4147-4150.

HASKELL, N. A., 1962. Crustal reflection of plane *P* and *SV* waves, *J. Geophys. Res.*, **67**, 4751-4767.

HASKELL, N. A., 1964. Total energy and energy spectral density of elastic wave radiation from propagating faults, *Bull. Seismol. Soc. Am.*, **54**, 1811-1841.

HEDAYATI, A., and T. HIRASAWA, 1966. Mechanism of the Hindu Kush Earthquake of Jan. 28, 1964, derived from *S* wave data: the use of *pP*-phase for the focal mechanism determination, *Bull. Earthquake Res. Inst. Tokyo Univ.*, **44**, 1419-1434.

HONDA, H., 1959. The elastic waves generated from a spherical source, *Sci. Rept. Tohoku Univ.*, **5**, **11**, 178-183.

HONDA, H., 1962. Earthquake mechanism and seismic waves, *Geophys. Notes, Fac. Sci., Tokyo Univ.*, **15**, 1-97.

ISACKS, B., and P. MOLNAR, 1969. Mantle earthquake mechanisms and the sinking of the lithosphere, *Nature*, **223**, 1121-1124.

ISACKS, B., J. OLIVER, and L. R. SYKES, 1968. Seismology and the new global tectonics, *J. Geophys. Res.*, **73**, 5855-5899.

KANAMORI, H., 1967. Attenuation of *P* waves in the upper and lower mantle, *Bull. Earthquake Res. Inst. Tokyo Univ.*, **45**, 299-312.

KNOPOFF, L., 1958. Energy release in earthquakes, *Geophys. J.*, **1**, 44-52.

KOVACH, R. L., and D. L. ANDERSON, 1964. Attenuation of shear waves in the upper and lower mantle, *Bull. Seismol. Soc. Am.*, **54**, 1855-1864.

MCKENZIE, D. P., 1969a. The relation between fault plane solutions for earthquakes and the directions of the principal stresses, *Bull. Seismol. Soc. Am.*, **59**, 591-601.

MCKENZIE, D. P., 1969b. Speculations on the consequences and causes of plate motions, *Geophys. J.*, **18**, 1-32.

MIKUMO, T., 1969. Long-period *P* waveforms and the source mechanism of intermediate earthquakes, *J. Phys. Earth*, **17**, 169-192.

OROWAN, E., 1961. Mechanism of seismic faulting; in Rock deformation, *Geol. Soc. Am., Memoir*, **79**.

OROWAN, E., 1965. Physics of the seismic source, *Boeing Sci. Trd. Lab. Seattle. Washington, D1-82-0471.*

RALEIGH, C. B., and M. S. PATERSON, 1965. Experimental deformation of serpentinite and its tectonic implications, *J. Geophys. Res.*, **70**, 3965-3985.

RANDALL, M. J., 1964. On the mechanism of earthquakes, *Bull. Seismol. Soc. Am.*, **54**, 1283-1289.

RANDALL, M. J., 1966. Seismic radiation from a sudden phase transition, *J. Geophys. Res.*, **71**, 5297-5302.

RANDALL, M. J., 1968. Relative sizes of multipolar components in deep earthquakes, *J. Geophys. Res.*, **73**, 6140-6142.

RITSEMA, A. R., 1958. $(i-\Delta)$—curves for bodily seismic waves of any focal depths, *Meteorol. and Geophys. Inst. Djakarta, Verhandelingen*, **54**, 1-10.

ROTHÉ, J. P., 1969. The seismicity of the earth 1953-1965, the United Nations Educational, Scientific and Cultural Organization.

SAVAGE, J. C., 1966. Radiation from a realistic model of faulting, *Bull. Seismol. Soc. Am.*, **56**, 577-592.

SAVAGE, J. C., 1969. Steketee's paradox, *Bull. Seismol. Soc. Am.*, **59**, 381-384.
SAVAGE, J. C., 1969. The mechanics of deep-focus faulting, *Tectonophys.*, **8**, 115-127.
SHIMAMURA, H., and R. SATO, 1965. Model experiments on body waves-travel times, amplitudes, wave forms and attenuation, *J. Phys. Earth*, **13**, 10-33.
TENG, T. L., and A. BEN-MENAHEM, 1965. Mechanism of deep earthquakes from spectrums of isolated body-wave signals, *J. Geophys. Res.*, **70**, 5157-5170.
VEDENSKAYA, A. A., 1959. The displacement field associated with discontinuities in an elastic medium, *Bull. Acad. Sci. USSR., Geophys. Ser., English Transl.* 357-362.
WALKER, C. T., and J. G. DENNIS, 1966. Explosive phase transitions in the earth's mantle, *Nature*, **209**, 182-183.
WUENSCHEL, P. C., 1965. Dispersive body waves—an experimental study, *Geophys.*, **30**, 539-551.
WYSS, M., and J. N. BRUNE, 1969. Shear stresses associated with earthquakes between 0 and 700 km depth (abstract), *Trans. Am. Geophys. Union*, **50**, 237.

38. 長周期 P 波および S 波より推定した深発地震の震源過程

地震研究所 深尾良夫

1964 年バンダ海で起った深さ 580 km の深発地震の震源過程を世界標準地震計観測網が記録した長周期 P 波および S 波を用いて調べた．この地震の 2 つの P 波節面は dip direction=319°, dip angle=45° および dip direction=180°, dip angle=53° で与えられる．S 波の遠方での波形が矩形で近似できると仮定して種々のパルス巾，震央距離に対して P 波理論記象を作った．その際，マントル，地殻および地震計を通過するときの波形への影響を考慮した．これらを実際の記録と比較して，もとの矩形波のパルス巾，T_s，を求めた．T_s の方位に関する著しい規則性より次の結論を得た．(1) 震源は球状ではなく面状であり，従って相転移モデルより断層モデルの方が適当である．(2) dip direction=319°, dip angle=45° の P 波節面が断層面である．(3) 断層面は円ではなく，slip 方向にのびた細長いものである．(4) 断層の巾は 15 km を越えず，恐らく 10 km 以下と思われる．(5) 地震は断層面全体にわたって殆ど同時に起ったと考えられる．この間約 2 秒である．普通の伝播性断層モデルでは結果を説明できない．(6) 断層の長さは約 40 km である．これらの結論は P 波の実際の波形とも矛盾しない．P 波理論記象と実際の記録との比較から地震モーメントは 5.8×10^{26} dyne cm と推定される．断層の巾を 8 km と仮定すると，断層面上でのくい違いの大きさ，stress drop および断層面が free になったと仮定したとき解放される弾性エネルギーは，それぞれ 150 cm, 290 bars および 7.0×10^{22} ergs となる．